



Nonlocal strain gradient forced vibrations of FG-GPLRC nanocomposite microbeams

Qiannan Wu¹ · Haohao Chen¹ · Wan Gao¹

Received: 14 May 2019 / Accepted: 4 June 2019 / Published online: 17 June 2019
© Springer-Verlag London Ltd., part of Springer Nature 2019

Abstract

In the current investigation, based upon the nonlocal strain gradient theory of elasticity, an inhomogeneous size-dependent beam model is formulated within the framework of a refined hyperbolic shear deformation beam theory. Thereafter, via the constructed nonlocal strain gradient refined beam model, the nonlinear primary resonance of laminated functionally graded graphene platelet-reinforced composite (FG-GPLRC) microbeams under external harmonic excitation is studied in the presence of the both hardening-stiffness and softening-stiffness size effects. The graphene platelets are randomly dispersed in each individual layer in such a way that the weight fraction of the reinforcement varies on the basis of different patterns of FG dispersion. Based upon the Halpin–Tsai micromechanical scheme, the effective material properties of laminated FG-GPLRC microbeams are achieved. By putting the Hamilton’s principle to use, the nonlocal strain gradient equations of motion are developed. After that, a numerical solving process using the generalized differential quadrature (GDQ) method together with the Galerkin technique is employed to obtain the nonlocal strain gradient frequency response and amplitude response associated with the nonlinear primary resonance of laminated FG-GPLRC microbeams. It is found that the nonlocality size effect leads to an increase in the peak of the jump phenomenon and the associated excitation frequency, while the strain gradient size dependency results in a reduction in both of them.

Keywords Nanocomposites · Multilayer functionally graded · Nonlinear resonance · Graphene platelets · Size effect

1 Introduction

The exceptional mechanical, electrical and thermal characteristics of graphene have led to attracting tremendous attention from the research community. Graphene-based nanocomposite materials can be one of the most promising applications of graphene nanosheets. Using graphene platelet (GPL) as composite nanofiller makes the enhancement of multifunctional property possible. Recently, some studies have been carried out to analyze the mechanical behavior of multilayer functional graded graphene platelet-reinforced composite (FG-GPLRC) structures. Yang et al. [1] reported the buckling and postbuckling response of laminated FG-GPLRC Timoshenko beams using the differential quadrature method. Song et al. [2] predicted the

free and forced vibrations of multilayer FG-GPLRC first-order shear deformable plates using the Navier solution. Feng et al. [3] investigated the nonlinear bending characteristic of laminated FG-GPLRC Timoshenko beams via the Ritz method. Wu et al. [4] examined the dynamic stability of laminated FG-GPLRC nanocomposite beams based on Bolotin’s method.

Due to the rapid advancement in materials science and technology, the miniaturized FG materials can provide a new opportunity for design of efficient micro- and nano-electromechanical systems and devices [5–7]. As a result, size dependency in mechanical behaviors of these small-scale structures is worth studying. In the last decade, several unconventional continuum theories of elasticity have been employed to study the size-dependent characteristics of microstructures [8–35].

Generally, in the previous investigations, it has been observed that the size effect in type of stress nonlocality has a softening-stiffness influence, while the strain gradient size dependency leads to a hardening-stiffness effect.

✉ Qiannan Wu
qiannanwoo@nuc.edu.cn

¹ School of Science, North University of China,
Taiyuan 030051, China

Accordingly, Lim et al. [36] proposed a more comprehensive size-dependent continuum theory namely nonlocal strain gradient elasticity which includes both softening and stiffening influences to describe the size dependency in a more accurate way. Afterwards, a few studies have been performed on the basis of nonlocal strain gradient elasticity theory. Li and Hu [37] reported the size-dependent critical buckling loads of nonlinear Euler–Bernoulli nanobeams based upon nonlocal strain gradient theory of elasticity. They also presented the size-dependent frequency of wave motion on fluid-conveying carbon nanotubes via nonlocal strain gradient theory [38]. Yang et al. [39] established a nonlocal strain gradient beam model to evaluate the critical voltages corresponding to pull-in instability FG carbon nanotube-reinforced actuators at nanoscale. Simsek [40] used the nonlocal strain gradient theory to capture the size effects on the nonlinear natural frequencies of FGM Euler–Bernoulli nanobeams. Sahmani and Aghdam [41–44] employed the theory of nonlocal strain gradient elasticity to analyze the nonlinear instability of micro/nanoshells under various types of loading condition. Li et al. [45] anticipated the size-dependent nonlinear free vibration response of porous nanobeams based on the nonlocal strain gradient Euler–Bernoulli beam model. Radwan and Sobhy [46] studied the nonlocal strain gradient dynamic deformation response of graphene sheets on a viscoelastic foundation under a time harmonic thermal load. Wang et al. [47] predicted the transverse-free vibrations of axially moving nanobeams on the basis of nonlocal strain gradient Euler–Bernoulli beam model. Sahmani and Aghdam [48–51] put the nonlocal strain gradient elasticity theory to use for size-dependent analysis of nonlinear mechanical behavior of GPLRC micro/nanostructures. Zeighampour et al. [52] examined the wave propagation in viscoelastic cylindrical nanoshells surrounded by an elastic medium via a developed nonlocal strain gradient shell model.

The main objective of this work is to analyze the size-dependent nonlinear primary resonance of harmonic excited FG-GPLRC laminated microbeams based upon the nonlocal strain gradient hyperbolic shear deformable beam model. With the aid of the Hamilton’s principle, the non-classical nonlinear differential equations of motion are constructed. On the basis of the Halpin–Tsai micromechanical scheme, the effective material properties of laminated FG-GPLRC microbeams are achieved. Thereafter, a numerical solution methodology using generalized differential quadrature method together with the Galerkin technique was reported and the nonlocal strain gradient frequency response and amplitude response associated with the primary resonance of FG-GPLRC laminated microbeams was obtained.

2 Nonlocal strain gradient refined beam model

Figure 1 illustrates a six-layer FG-GPLRC microbeam with length L , width b , thickness h and the attached coordinate system. The thicknesses of all six layers are the same equal to $h_l = h/6$. Based upon the related dispersion pattern, the weight fraction of GPLs varies layer by layer of the laminated microbeam. In accordance with Fig. 1, three different patterns of GPL dispersion namely X-GPLRC, O-GPLRC and A-GPLRC are taken into consideration together with the uniform one (U-GPLRC). As a consequence, for each type of GPL dispersion pattern, the GPL volume fraction associated with k -th layer can be given as [6],

$$\begin{aligned}
 U - \text{GPLRC} : V_{\text{GPL}}^{(k)} &= V_{\text{GPL}}^* \\
 X - \text{GPLRC} : V_{\text{GPL}}^{(k)} &= 2V_{\text{GPL}}^* (|2k - n_L - 1|/n_L), \\
 O - \text{GPLRC} : V_{\text{GPL}}^{(k)} &= 2V_{\text{GPL}}^* (1 - (|2k - n_L - 1|/n_L)), \\
 A - \text{GPLRC} : V_{\text{GPL}}^{(k)} &= V_{\text{GPL}}^* ((2k - 1)/n_L),
 \end{aligned} \tag{1}$$

in which n_L represents the total number of layers and V_{GPL}^* stands for the total GPL volume fraction of the laminated micro/nanobeam as shown below:

$$V_{\text{GPL}}^* = \frac{W_{\text{GPL}}}{W_{\text{GPL}} + \left(\frac{\rho_{\text{GPL}}}{\rho_m}\right)(1 - W_{\text{GPL}})}, \tag{2}$$

where ρ_{GPL} and ρ_m in order denote the mass densities associated with GPLs and the polymer matrix of the laminated microbeam made from the FG-GPLRC nanocomposite. Also, W_{GPL} is the GPL weight fraction.

With the aid of the Halpin–Tsai scheme [53], the Young’s modulus relevant to k -th layer of the FG-GPLRC containing randomly oriented reinforcements can be extracted as,

$$E^{(k)} = \left(\frac{3}{8} \frac{1 + \lambda_L \eta_L V_{\text{GPL}}^{(k)}}{1 - \eta_L V_{\text{GPL}}^{(k)}} + \frac{5}{8} \frac{1 + \lambda_T \eta_T V_{\text{GPL}}^{(k)}}{1 - \eta_T V_{\text{GPL}}^{(k)}} \right) E_m, \tag{3}$$

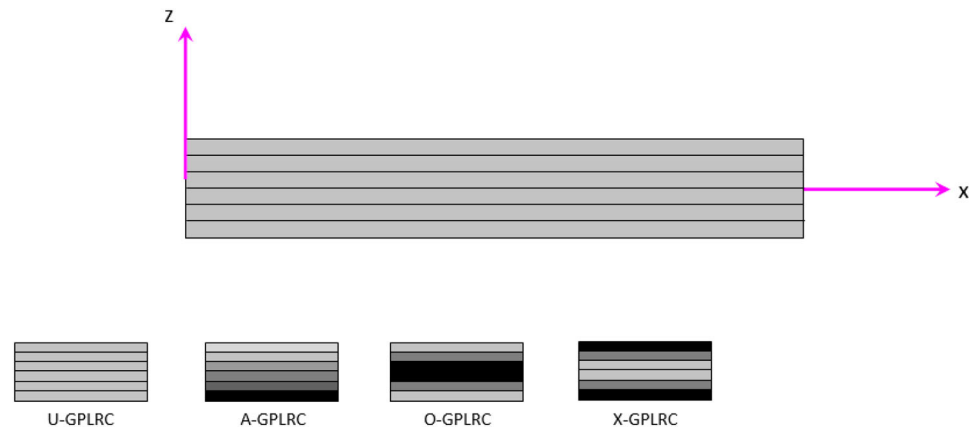
in which E_m denotes the Young’s modulus of the polymer matrix, and,

$$\begin{aligned}
 \eta_L &= \frac{\frac{E_{\text{GPL}}}{E_m} - 1}{\frac{E_{\text{GPL}}}{E_m} + \lambda_L}, & \eta_T &= \frac{\frac{E_{\text{GPL}}}{E_m} - 1}{\frac{E_{\text{GPL}}}{E_m} + \lambda_T}, & \lambda_L &= \frac{2L_{\text{GPL}}}{h_{\text{GPL}}}, \\
 \lambda_T &= \frac{2b_{\text{GPL}}}{h_{\text{GPL}}},
 \end{aligned} \tag{4}$$

where E_{GPL} , L_{GPL} , b_{GPL} , h_{GPL} are, respectively, the Young’s modulus, length, width and thickness of GPL nanofillers.

Additionally, on the basis of the rule of mixture [54], the Poisson’s ratio and mass density of the k -th layer of the FG-GPLRC laminated microbeam can be obtained as,

Fig. 1 A FG-GPLRC laminated micro/nanobeam with various GPL distributions



$$\begin{aligned}
 \nu^{(k)} &= \nu_m \left(1 - V_{\text{GPL}}^{(k)}\right) + \nu_{\text{GPL}} V_{\text{GPL}}^{(k)}, \\
 \rho^{(k)} &= \rho_m \left(1 - V_{\text{GPL}}^{(k)}\right) + \rho_{\text{GPL}} V_{\text{GPL}}^{(k)},
 \end{aligned}
 \tag{5}$$

where ν_m and ρ_m stand for the Poisson’s ratio and mass density of the polymer matrix, respectively. Also, ν_{GPL} and ρ_{GPL} denote, respectively, the Poisson’s ratio and mass density of GPL reinforcements.

Based upon the hyperbolic shear deformation beam theory, the displacement field along different coordinate directions can be written as,

$$u_x(x, z, t) = u(x, t) - zw_{,x}(x, t) + [z \cosh(1/2) - h \sinh(z/h)]\psi(x, t),
 \tag{6a}$$

$$u_z(x, z, t) = w(x, t),
 \tag{6b}$$

where u and w in order are the displacement components of the FG-GPLRC laminated microbeam along x - and z -axis. Additionally, ψ represents the rotation with respect to the cross-section of the microbeam at neutral plane, normal about y -axis.

Consequently, the non-zero strain components are derived as,

$$\begin{Bmatrix} \varepsilon_{xx} \\ \gamma_{xz} \end{Bmatrix} = \begin{Bmatrix} u_{,x} + \left(\frac{1}{2}\right)w_{,x}^2 - zw_{,xx} + \left[z \cosh\left(\frac{1}{2}\right) - h \sinh\left(\frac{z}{h}\right)\right]\psi_{,x} \\ \left[\cosh\left(\frac{1}{2}\right) - \cosh\left(\frac{z}{h}\right)\right]\psi \end{Bmatrix}.
 \tag{7}$$

As it has been reported previously, the nonlocal elasticity theory and strain gradient elasticity theory do not consider size effect comprehensively. The nonlocal theory cannot take the higher-order stresses into account. On the other hand, the strain gradient theory has the capability to consider only local higher-order strain gradients. Motivated by this fact, Lim et al. [36] proposed a combination of these theories namely nonlocal strain gradient elasticity theory which assess small-scale effects more reasonably. Accordingly, the total nonlocal strain gradient stress tensor

A for a beam-type structure can be defined as seen below [36],

$$A_{xx} = \sigma_{xx} - \sigma_{xx,x}^*,
 \tag{8a}$$

$$A_{xz} = \sigma_{xz} - \sigma_{xz,x}^*,
 \tag{8b}$$

where σ and σ^* are the stress and higher-order stress tensors.

In accordance with the method of Eringen, the constitutive equation relevant to the total nonlocal strain gradient stress tensor of a FG-GPLRC laminated microbeam can be derived as,

$$\begin{Bmatrix} A_{xx} - \mu^2 A_{xx,xx} \\ A_{xz} - \mu^2 A_{xz,xx} \end{Bmatrix}_{(k)} = \begin{bmatrix} Q_{11}^{(k)} & 0 \\ 0 & Q_{44}^{(k)} \end{bmatrix} \begin{Bmatrix} \varepsilon_{xx} - l^2 \varepsilon_{xx,xx} \\ \varepsilon_{xz} - l^2 \varepsilon_{xz,xx} \end{Bmatrix}_{(k)},
 \tag{9}$$

in which,

$$Q_{11}^{(k)} = \frac{E^{(k)}}{1 - (\nu^{(k)})^2}, \quad Q_{44}^{(k)} = \frac{E^{(k)}}{2(1 + \nu^{(k)})},
 \tag{10}$$

and μ and l in order are the nonlocal parameter and strain gradient parameter. Thereafter, the nonlocal strain gradient constitutive relations for a hyperbolic shear deformable FG-GPLRC laminated microbeam can be expressed as,

$$\begin{Bmatrix} A_{xx} - \mu^2 A_{xx,xx} \\ A_{xz} - \mu^2 A_{xz,xx} \end{Bmatrix}_{(k)} = \begin{bmatrix} Q_{11}^{(k)} & 0 \\ 0 & Q_{44}^{(k)} \end{bmatrix} \begin{Bmatrix} u_{,x} + \left(\frac{1}{2}\right)(w_{,x})^2 - zw_{,xx} + \left[z \cosh\left(\frac{1}{2}\right) - h \sinh\left(\frac{z}{h}\right)\right]\psi_{,x} \\ \left[\cosh\left(\frac{1}{2}\right) - \cosh\left(\frac{z}{h}\right)\right]\psi \end{Bmatrix}_{(k)} - l^2 \begin{Bmatrix} u_{,xxx} + w_{,x}w_{,xxx} + w_{,xx}^2 - zw_{,xxx} + \left[z \cosh\left(\frac{1}{2}\right) - h \sinh\left(\frac{z}{h}\right)\right]\psi_{,xxx} \\ \left[\cosh\left(\frac{1}{2}\right) - \cosh\left(\frac{z}{h}\right)\right]\psi_{,xx} \end{Bmatrix}_{(k)}.
 \tag{11}$$

Therefore, within the framework of the nonlocal strain gradient hyperbolic shear deformable beam model, the

total strain energy of a FG-GPLRC laminated microbeam can be written as,

$$\begin{aligned} \Pi_s &= \frac{1}{2} \int_0^L \int_S \left\{ \sigma_{ij} \varepsilon_{ij} + \sigma_{ij}^* \nabla \varepsilon_{ij} \right\} dS dx \\ &= \frac{1}{2} \int_0^L \left\{ N_{xx} \left[u_{,x} + \left(\frac{1}{2} \right) w_{,x}^2 \right] - M_{xx} w_{,xx} + R_{xx} \psi_{,x} + Q_x \psi \right\} dx, \end{aligned} \tag{12}$$

where S represents the cross-sectional area of the FG-GPLRC laminated microbeam. Also, the stress resultants can be achieved in the following forms,

$$\begin{aligned} N_{xx} - \mu^2 N_{xx,xx} &= A_{11}^* \left[u_{,x} + \left(\frac{1}{2} \right) w_{,x}^2 - l^2 (u_{,xxx} + w_{,x} w_{,xxx} + w_{,xx}^2) \right] \\ &\quad + B_{11}^* (-w_{,xx} + l^2 w_{,xxxx}) + C_{11}^* (\psi_{,x} - l^2 \psi_{,xxx}) \\ M_{xx} - \mu^2 M_{xx,xx} &= B_{11}^* \left[u_{,x} + \left(\frac{1}{2} \right) w_{,x}^2 - l^2 (u_{,xxx} + w_{,x} w_{,xxx} + w_{,xx}^2) \right] \\ &\quad + D_{11}^* (-w_{,xx} + l^2 w_{,xxxx}) + F_{11}^* (\psi_{,x} - l^2 \psi_{,xxx}) \\ R_{xx} - \mu^2 R_{xx,xx} &= C_{11}^* \left[u_{,x} + \left(\frac{1}{2} \right) w_{,x}^2 - l^2 (u_{,xxx} + w_{,x} w_{,xxx} + w_{,xx}^2) \right] \\ &\quad + F_{11}^* (-w_{,xx} + l^2 w_{,xxxx}) + G_{11}^* (\psi_{,x} - l^2 \psi_{,xxx}) \\ Q_x - \mu^2 Q_{x,xx} &= A_{44}^* (\psi - l^2 \psi_{,xx}), \end{aligned} \tag{13}$$

in which,

$$\begin{aligned} \{N_{xx}, M_{xx}, R_{xx}\} &= b \sum_{k=1}^{n_L} \left(\int_{z_{k-1}}^{z_k} A_{xx}^{(k)} \left\{ 1, z, z \cosh \left(\frac{1}{2} \right) - h \sinh \left(\frac{z}{h} \right) \right\} dz \right) \\ Q_x &= b \sum_{k=1}^{n_L} \int_{z_{k-1}}^{z_k} A_{xz}^{(k)} \left\{ \cosh \left(\frac{1}{2} \right) - \cosh \left(\frac{z}{h} \right) \right\} dz, \end{aligned} \tag{14}$$

and,

$$\begin{aligned} \{A_{11}^*, B_{11}^*, C_{11}^*\} &= b \sum_{k=1}^{n_L} \left(Q_{11}^{(k)} \int_{z_{k-1}}^{z_k} \left\{ 1, z, z \cosh \left(\frac{1}{2} \right) - h \sinh \left(\frac{z}{h} \right) \right\} dz \right) \\ \{D_{11}^*, F_{11}^*, G_{11}^*\} &= b \sum_{k=1}^{n_L} \left(Q_{11}^{(k)} \int_{z_{k-1}}^{z_k} \left\{ z^2, z^2 \cosh \left(\frac{1}{2} \right) - zh \sinh \left(\frac{z}{h} \right), \right. \right. \\ &\quad \left. \left. \left[z \cosh \left(\frac{1}{2} \right) - h \sinh \left(\frac{z}{h} \right) \right]^2 \right\} dz \right) \\ A_{44}^* &= b \sum_{k=1}^{n_L} \left(Q_{44}^{(k)} \int_{z_{k-1}}^{z_k} \left\{ \cosh \left(\frac{1}{2} \right) - \cosh \left(\frac{z}{h} \right) \right\} dz \right). \end{aligned} \tag{15}$$

Furthermore, the kinetic energy of a FG-GPLRC laminated microbeam modeled via the nonlocal strain gradient hyperbolic shear deformable beam model can be expressed as,

$$\begin{aligned} \Pi_T &= \frac{1}{2} \int_0^L \int_S \rho \left\{ (u_{x,t})^2 + (u_{z,t})^2 \right\} dS dx \\ &= \frac{1}{2} \int_0^L \left\{ I_0 (u_{,t})^2 - 2I_1 u_{,t} w_{,xt} + 2I_2 u_{,t} \psi_{,t} + I_3 (w_{,xt})^2 \right. \\ &\quad \left. - 2I_4 w_{,xt} \psi_{,t} + I_5 (\psi_{,t})^2 + I_0 (w_{,t})^2 \right\} dx, \end{aligned} \tag{16}$$

where,

$$\begin{aligned} \{I_0, I_1, I_2\} &= b \sum_{k=1}^{n_L} \left(\rho^{(k)} \int_{z_{k-1}}^{z_k} \left\{ 1, z, z \cosh \left(\frac{1}{2} \right) - h \sinh \left(\frac{z}{h} \right) \right\} dz \right) \\ \{I_3, I_4, I_5\} &= b \sum_{k=1}^{n_L} \left(\rho^{(k)} \int_{z_{k-1}}^{z_k} \left\{ z^2, z^2 \cosh \left(\frac{1}{2} \right) - zh \sinh \left(\frac{z}{h} \right), \right. \right. \\ &\quad \left. \left. \left[z \cosh \left(\frac{1}{2} \right) - h \sinh \left(\frac{z}{h} \right) \right]^2 \right\} dz \right). \end{aligned} \tag{17}$$

Additionally, the work done by the transverse force q can be defined as follows:

$$\Pi_P = \int_0^L q(x, t) w dx. \tag{18}$$

Thereby, using the Hamilton’s principle, the governing differential equations in terms of the stress resultants can be derived as,

$$N_{xx,x} = I_0 u_{,tt} - I_1 w_{,xxt} + I_2 \psi_{,tt}, \tag{19a}$$

$$M_{xx,xx} + (N_{xx} w_{,x})_{,x} + q = I_0 w_{,tt} + I_1 u_{,xtt} - I_3 w_{,xxtt} + I_4 \psi_{,xtt}, \tag{19b}$$

$$R_{xx,x} - Q_x = I_2 u_{,tt} - I_4 w_{,xtt} + I_5 \psi_{,xtt} \tag{19c}$$

Thereafter, by inserting Eqs. (13) in (19a, 19b), the nonlinear size-dependent equations of motion can be rewritten as,

$$\begin{aligned} A_{11}^* [u_{,xx} + w_{,x} w_{,xx} - l^2 (u_{,xxxx} + 3w_{,xx} w_{,xxx} + w_{,x} w_{,xxxx})] \\ + B_{11}^* (-w_{,xxx} + l^2 w_{,xxxx}) + C_{11}^* (\psi_{,xx} - l^2 \psi_{,xxxx}) \\ = I_0 (u_{,tt} - \mu^2 u_{,xtt}) - I_1 (w_{,xxt} - \mu^2 w_{,xxxxt}) + I_2 (\psi_{,tt} - \mu^2 \psi_{,xtt}), \end{aligned} \tag{20a}$$

$$\begin{aligned}
 & B_{11}^* \left[u_{,xxx} + w_{,xx}^2 + w_{,x}w_{,xxx} - l^2 \right. \\
 & \left. \left(u_{,xxxx} + 3w_{,xxx}^2 + 4w_{,xx}w_{,xxxx} + w_{,x}w_{,xxxx} \right) \right] \\
 & + D_{11}^* (-w_{,xxx} + l^2 w_{,xxxx}) + F_{11}^* (\psi_{,xxx} - l^2 \psi_{,xxxx}) \\
 & + A_{11}^* \Gamma_1 - l^2 A_{11}^* \Gamma_2 - \mu^2 A_{11}^* \Gamma_3 + \mu^2 l^2 A_{11}^* \Gamma_4 - B_{11}^* \Gamma_5 \\
 & + l^2 B_{11}^* \Gamma_6 + \mu^2 B_{11}^* \Gamma_7 - \mu^2 l^2 B_{11}^* \Gamma_8 + C_{11}^* \Gamma_9 \\
 & - l^2 C_{11}^* \Gamma_{10} - \mu^2 C_{11}^* \Gamma_{11} + \mu^2 l^2 C_{11}^* \Gamma_{12} \\
 & = I_0 (w_{,tt} - \mu^2 w_{,xxt}) + I_1 (u_{,xtt} - \mu^2 u_{,xxtt}) \\
 & - I_3 (w_{,xxt} - \mu^2 w_{,xxxxt}) \\
 & + I_4 (\psi_{,xtt} - \mu^2 \psi_{,xxxxt}) - \varrho + \mu^2 \varrho_{,xx}, \tag{20b}
 \end{aligned}$$

$$\begin{aligned}
 & C_{11}^* [u_{,xx} + w_{,x}w_{,xx} - l^2 (u_{,xxx} + 3w_{,xx}w_{,xxx} + w_{,x}w_{,xxxx})] \\
 & + F_{11}^* (-w_{,xxx} + l^2 w_{,xxxx}) \\
 & + G_{11}^* (\psi_{,xx} - l^2 \psi_{,xxx}) - A_{44}^* (\psi - l^2 \psi_{,xx}) \\
 & = I_2 (u_{,tt} - \mu^2 u_{,xxt}) - I_4 (w_{,xtt} - \mu^2 w_{,xxxxt}) \\
 & + I_5 (\psi_{,tt} - \mu^2 \psi_{,xxxxt}), \tag{20c}
 \end{aligned}$$

in which,

$$\begin{aligned}
 \Gamma_1 &= u_{,xx}w_{,x} + u_{,x}w_{,xx} + (3/2)w_{,xx}w_{,x}^2 \\
 \Gamma_2 &= u_{,xxx}w_{,x} + u_{,xx}w_{,xx} + 4w_{,x}w_{,xx}w_{,xxx} \\
 &+ (w_{,xx} + w_{,xxx})w_{,x}^2 \\
 \Gamma_3 &= u_{,xxx}w_{,x} + 3u_{,xx}w_{,xx} + 3u_{,xx}w_{,xxx} + u_{,x}w_{,xxxx} \\
 &+ 3w_{,xx}^3 + 9w_{,x}w_{,xx}w_{,xxx} + (3/2)w_{,xx}^2w_{,xxx} \\
 \Gamma_4 &= u_{,xxxx}w_{,x} + 3u_{,xxx}w_{,xx} + 3u_{,xxx}w_{,xxx} + u_{,xx}w_{,xxxx} \\
 &+ 10w_{,xxx}w_{,xx}^2 + 12w_{,xx}w_{,xxx}^2 \\
 &+ 14w_{,x}w_{,xx}w_{,xxx} + 8w_{,x}w_{,xx}w_{,xxxx} + 6w_{,x}w_{,xx}w_{,xxx} \\
 &+ (w_{,xxx} + w_{,xxxx})w_{,x}^2 + 2w_{,xx}^3 \\
 \Gamma_5 &= w_{,x}w_{,xxx} + w_{,xx}^2 \\
 \Gamma_6 &= w_{,xx}w_{,xxx} + w_{,x}w_{,xxxx} \\
 \Gamma_7 &= 3w_{,xxx}^2 + 4w_{,xx}w_{,xxxx} + w_{,x}w_{,xxxx} \\
 \Gamma_8 &= w_{,xxxx}^2 + 3w_{,xxx}w_{,xxxx} + 3w_{,xx}w_{,xxxx} + w_{,x}w_{,xxxx} \\
 \Gamma_9 &= w_{,xx}\psi_{,x} + w_{,x}\psi_{,xx} \\
 \Gamma_{10} &= w_{,xx}\psi_{,xxx} + w_{,x}\psi_{,xxxx} \\
 \Gamma_{11} &= w_{,xxx}\psi_{,x} + 3w_{,xxx}\psi_{,xx} + 3w_{,xx}\psi_{,xxx} + w_{,x}\psi_{,xxxx} \\
 \Gamma_{12} &= w_{,xxxx}\psi_{,xxx} + 3w_{,xxx}\psi_{,xxxx} + 3w_{,xx}\psi_{,xxxx} + w_{,x}\psi_{,xxxx}. \tag{21}
 \end{aligned}$$

To perform the numerical solving process in a more general form, the following dimensionless parameters are taken into consideration,

$$\begin{aligned}
 X &= \frac{x}{L}, \quad U = \frac{u}{h}, \quad W = \frac{w}{h}, \quad \Psi = \psi, \\
 \eta_1 &= \frac{l}{L}, \quad \eta_2 = \frac{\mu}{L}, \quad \beta = \frac{h}{L} \\
 T &= \frac{t}{L} \sqrt{\frac{A_{11}^*}{I_0}}, \quad \{a_{11}^*, a_{44}^*, b_{11}^*, c_{11}^*, d_{11}^*, f_{11}^*, g_{11}^*\} \\
 &= \left\{ \frac{A_{11}^*}{A_{11}^*}, \frac{A_{44}^*}{A_{11}^*}, \frac{B_{11}^*}{A_{11}^* h}, \frac{C_{11}^*}{A_{11}^* h}, \frac{D_{11}^*}{A_{11}^* h^2}, \frac{F_{11}^*}{A_{11}^* h^2}, \frac{G_{11}^*}{A_{11}^* h^2} \right\} \\
 \{I_0^*, I_1^*, I_2^*, I_3^*, I_4^*, I_5^*\} &= \left\{ \frac{I_0}{I_0}, \frac{I_1}{I_0 h}, \frac{I_2}{I_0 h}, \frac{I_3}{I_0 h^2}, \frac{I_4}{I_0 h^2}, \frac{I_5}{I_0 h^2} \right\}, \quad \mathcal{Q} = \frac{\varrho L^2}{A_{11}^* h}. \tag{22}
 \end{aligned}$$

As a result, the dimensionless form of the size-dependent nonlinear governing differential equations of motion can be expressed as,

$$\begin{aligned}
 & a_{11}^* [U_{,XX} + \beta W_{,X}W_{,XX} - \eta_1^2 (U_{,XXXX} + 3\beta W_{,XX}W_{,XXX} \\
 & + \beta W_{,X}W_{,XXX})] - b_{11}^* (W_{,XXX} - \eta_1^2 W_{,XXXX}) \\
 & + c_{11}^* (\Psi_{,XX} - \eta_1^2 \Psi_{,XXX}) \\
 & = I_0^* (U_{,TT} - \eta_2^2 U_{,XXT}) - I_1^* (W_{,XXT} - \eta_2^2 W_{,XXXXT}) \\
 & + I_2^* (\Psi_{,TT} - \eta_2^2 \Psi_{,XXT}), \tag{23a}
 \end{aligned}$$

$$\begin{aligned}
 & b_{11}^* [U_{,XXX} + \beta W_{,XX}^2 + \beta W_{,X}W_{,XXX} \\
 & - \eta_1^2 (U_{,XXXX} + 3\beta W_{,XX}^2 + 4\beta W_{,XX}W_{,XXX} + \beta W_{,X}W_{,XXXX})] \\
 & - a_{11}^* (W_{,XXXX} - \eta_1^2 W_{,XXXX}) + f_{11}^* (\Psi_{,XXX} - \eta_1^2 \Psi_{,XXXX}) \\
 & + a_{11}^* \tilde{\Gamma}_1 - \eta_1^2 a_{11}^* \tilde{\Gamma}_2 - \eta_2^2 a_{11}^* \tilde{\Gamma}_3 + \eta_2^2 \eta_1^2 a_{11}^* \tilde{\Gamma}_4 - b_{11}^* \tilde{\Gamma}_5 \\
 & + \eta_1^2 b_{11}^* \tilde{\Gamma}_6 + \eta_2^2 b_{11}^* \tilde{\Gamma}_7 - \eta_2^2 \eta_1^2 b_{11}^* \tilde{\Gamma}_8 + c_{11}^* \tilde{\Gamma}_9 \\
 & - \eta_1^2 c_{11}^* \tilde{\Gamma}_{10} - \eta_2^2 c_{11}^* \tilde{\Gamma}_{11} + \eta_2^2 \eta_1^2 c_{11}^* \tilde{\Gamma}_{12} \\
 & = I_0^* (W_{,TT} - \eta_2^2 W_{,XXT}) + I_1^* (U_{,XTT} - \eta_2^2 U_{,XXXXT}) \\
 & - I_3^* (W_{,XXT} - \eta_2^2 W_{,XXXXT}) \\
 & + I_4^* (\Psi_{,XTT} - \eta_2^2 \Psi_{,XXXXT}) - \mathcal{Q} + \eta_2^2 \mathcal{Q}_{,XX}, \tag{23b}
 \end{aligned}$$

$$\begin{aligned}
 & c_{11}^* [U_{,XX} + \beta W_{,X}W_{,XX} - \eta_1^2 (U_{,XXXX} + 3\beta W_{,XX}W_{,XXX} \\
 & + \beta W_{,X}W_{,XXX})] - f_{11}^* (W_{,XXX} - \eta_1^2 W_{,XXXX}) \\
 & + g_{11}^* (\Psi_{,XX} - \eta_1^2 \Psi_{,XXX}) - a_{44}^* (\Psi - \eta_1^2 \Psi_{,XX}) \\
 & = I_2^* (U_{,TT} - \eta_2^2 U_{,XXT}) - I_4^* (W_{,XTT} - \eta_2^2 W_{,XXXXT}) \\
 & + I_5^* (\Psi_{,TT} - \eta_2^2 \Psi_{,XXT}), \tag{23c}
 \end{aligned}$$

where,

$$\begin{aligned}
 \tilde{T}_1 &= \beta U_{,xx} W_{,x} + \beta U_{,x} W_{,xx} + (3/2)\beta^2 W_{,xx} W_x^2 \\
 \tilde{T}_2 &= \beta U_{,xxxx} W_{,x} + \beta U_{,xxx} W_{,xx} + 4\beta^2 W_{,x} W_{,xx} W_{,xxx} \\
 &\quad + \beta^2 (W_{,xx} + W_{,xxxx}) W_x^2 \\
 \tilde{T}_3 &= \beta [U_{,xxxx} W_{,x} + 3U_{,xxx} W_{,xx} + 3U_{,xx} W_{,xxx} + U_{,x} W_{,xxxx}] \\
 &\quad + \beta^2 [3W_{,xx}^3 + 9W_{,x} W_{,xx} W_{,xxx} + (3/2)W_x^2 W_{,xxxx}] \\
 \tilde{T}_4 &= \beta [U_{,xxxxx} W_{,x} + 3U_{,xxxx} W_{,xx} + 3U_{,xxx} W_{,xxx} + U_{,xx} W_{,xxxx}] \\
 &\quad + \beta^2 [10W_{,xxxx} W_{,xx}^2 + 12W_{,xx} W_{,xxx}^2 \\
 &\quad + 14W_{,x} W_{,xxx} W_{,xxxx} + 8W_{,x} W_{,xx} W_{,xxxxx} + 6W_{,x} W_{,xx} W_{,xxx} \\
 &\quad + (W_{,xxxx} + W_{,xxxxx}) W_x^2 + 2W_{,xx}^3] \\
 \tilde{T}_5 &= \beta W_{,x} W_{,xxx} + \beta W_{,xx}^2 \\
 \tilde{T}_6 &= \beta W_{,xx} W_{,xxxx} + \beta W_{,x} W_{,xxxxx} \\
 \tilde{T}_7 &= 3\beta W_{,xxx}^2 + 4\beta W_{,xx} W_{,xxxx} + \beta W_{,x} W_{,xxxxx} \\
 \tilde{T}_8 &= \beta W_{,xxxx}^2 + 3\beta W_{,xxx} W_{,xxxxx} + 3\beta W_{,xx} W_{,xxxxxx} + \beta W_{,x} W_{,xxxxxxx} \\
 \tilde{T}_9 &= W_{,xx} \Psi_{,x} + W_{,x} \Psi_{,xx} \\
 \tilde{T}_{10} &= W_{,xx} \Psi_{,xxx} + W_{,x} \Psi_{,xxxx} \\
 \tilde{T}_{11} &= W_{,xxxx} \Psi_{,x} + 3W_{,xxx} \Psi_{,xx} + 3W_{,xx} \Psi_{,xxx} + W_{,x} \Psi_{,xxxx} \\
 \tilde{T}_{12} &= W_{,xxxx} \Psi_{,xxx} + 3W_{,xxx} \Psi_{,xxxx} + 3W_{,xx} \Psi_{,xxxxx} + W_{,x} \Psi_{,xxxxxx}.
 \end{aligned}
 \tag{24}$$

3 Numerical solution methodology

Herein, to capture the nonlinear nonlocal strain gradient frequency of a FG-GPLRC microbeam, a solving process on the basis of the GDQ numerical method is utilized [55]. Based upon the Chebyshev–Gauss–Lobatto scheme, a set of mesh points within X domain can be obtained as,

$$X_i = (1/2)[1 - \cos(\pi(i - 1)/(N - 1))], \quad i = 1, 2, \dots, N.
 \tag{25}$$

Consequently, the discretized nonlinear governing equations of motion can be written in terms of mass matrix, damping matrix and stiffness matrix as below,

$$\mathcal{M}\ddot{\mathbf{p}} + \mathcal{C}\dot{\mathbf{p}} + \mathcal{K}_L \mathbf{p} + \mathcal{K}_N = \mathcal{Q} \cos(\Omega T).
 \tag{26}$$

The derivative operators corresponding to each order can be introduced as,

$$\mathcal{D}_{ij}^r = \begin{cases} I_X & r = 0 \\ \frac{\prod_{j=1, j \neq i}^N (X_k - X_j)}{(X_i - X_j) \prod_{i=1, i \neq j}^N (X_j - X_i)} & r = 1, i, j = 1, 2, \dots, N \\ r \left(\mathcal{D}_{ij}^1 \mathcal{D}_{ii}^{r-1} - \frac{\mathcal{D}_{ij}^{r-1}}{(X_i - X_j)} \right) & r = 2, 3, \dots, N - 1, i, j = 1, 2, \dots, N \\ - \sum_{i=1, i \neq j}^N \mathcal{D}_{ij}^r & r = 1, 2, \dots, N - 1, i, j = 1, 2, \dots, N \end{cases}
 \tag{27}$$

where I_X represents the identity matrix.

Also, the time derivative operator corresponding to each order can be introduced explicitly in the following matrix forms,

$$\mathcal{D}_T^{(1)} = \mathbb{A}_{ij} \quad \text{where} \quad \begin{cases} \mathbb{A}_{1,1} = 0 \\ \mathbb{A}_{i,1} = (-1)^{i-1} \cot \left[\frac{\pi(i-1)}{N_t} \right] \\ \mathbb{A}_{i,j} = (-1)^{N_t-j+1} \cot \left[\frac{\pi(N_t-j+1)}{N_t} \right] \\ \mathbb{A}_{i+1,j+1} = \mathbb{A}_{ij} \end{cases} \quad i, j = 2, 3, \dots, N_t,
 \tag{28}$$

$$\mathcal{D}_T^{(2)} = \mathbb{B}_{ij} \quad \text{where} \quad \begin{cases} \mathbb{B}_{1,1} = -\frac{N_t^2}{12} - \frac{1}{6} \\ \mathbb{B}_{i,1} = \frac{(-1)^{i-1}}{2 \sin^2 \left[\frac{\pi(i-1)}{N_t} \right]} \\ \mathbb{B}_{i,j} = \frac{(-1)^{N_t-j+1}}{2 \sin^2 \left[\frac{\pi(N_t-j+1)}{N_t} \right]} \\ \mathbb{B}_{i+1,j+1} = \mathbb{B}_{ij} \end{cases} \quad i, j = 2, 3, \dots, N_t,
 \tag{29}$$

4 Numerical results and discussion

On the basis of the developed nonlocal strain gradient beam model, the size-dependent frequency response and amplitude response associated with the primary resonance of harmonic excited FG-GPLRC laminated microbeams are predicted. In the preceding numerical results, the damping parameter is assumed as $\mathcal{C} = 0.02$. Also, the geometric parameters of the FG-GPLRC laminated microbeams are selected as $h = 24$ nm for $n_L = 6$ and $b = h$, $L = 20h$, $h_{GPL} = 0.3$ nm, $L_{GPL} = 5$ nm, and $b_{GPL} = 2.5$ nm. In addition, ω_L stands for the linear natural frequency of the FG-GPLRC laminated microbeam. The material properties of the polymer matrix and GPL reinforcements are tabulated in Table 1.

Herein, the validity of the given solution is checked. To this end, by ignoring the strain gradient terms, the nonlocal natural frequencies of a simply supported carbon nanotube with different slenderness ratios are calculated and compared with those presented by Sahmani and Ansari [58] using the GDQ method and molecular dynamics

Table 1 Material properties of the polymer matrix and GPL reinforcements [56, 57]

E_{GPL} (TPa)	1.01
ν_{GPL}	0.186
ρ_{GPL} (kg/m ³)	1062.5
E_m (GPa)	3
ν_m	0.34
ρ_m (kg/m ³)	1200

Table 2 Comparison of natural frequencies of simply supported carbon nanotubes obtained by the nonlocal beam model and molecular dynamics simulations (THz)

Length-to-diameter ratio of carbon nanotube	Results of molecular dynamics simulation [58]	Results of GDQ method [58]	Results of the present solution methodology
24.5	0.0519	0.0521	0.0521
31.6	0.0358	0.0357	0.0357
39.1	0.0259	0.0259	0.0259

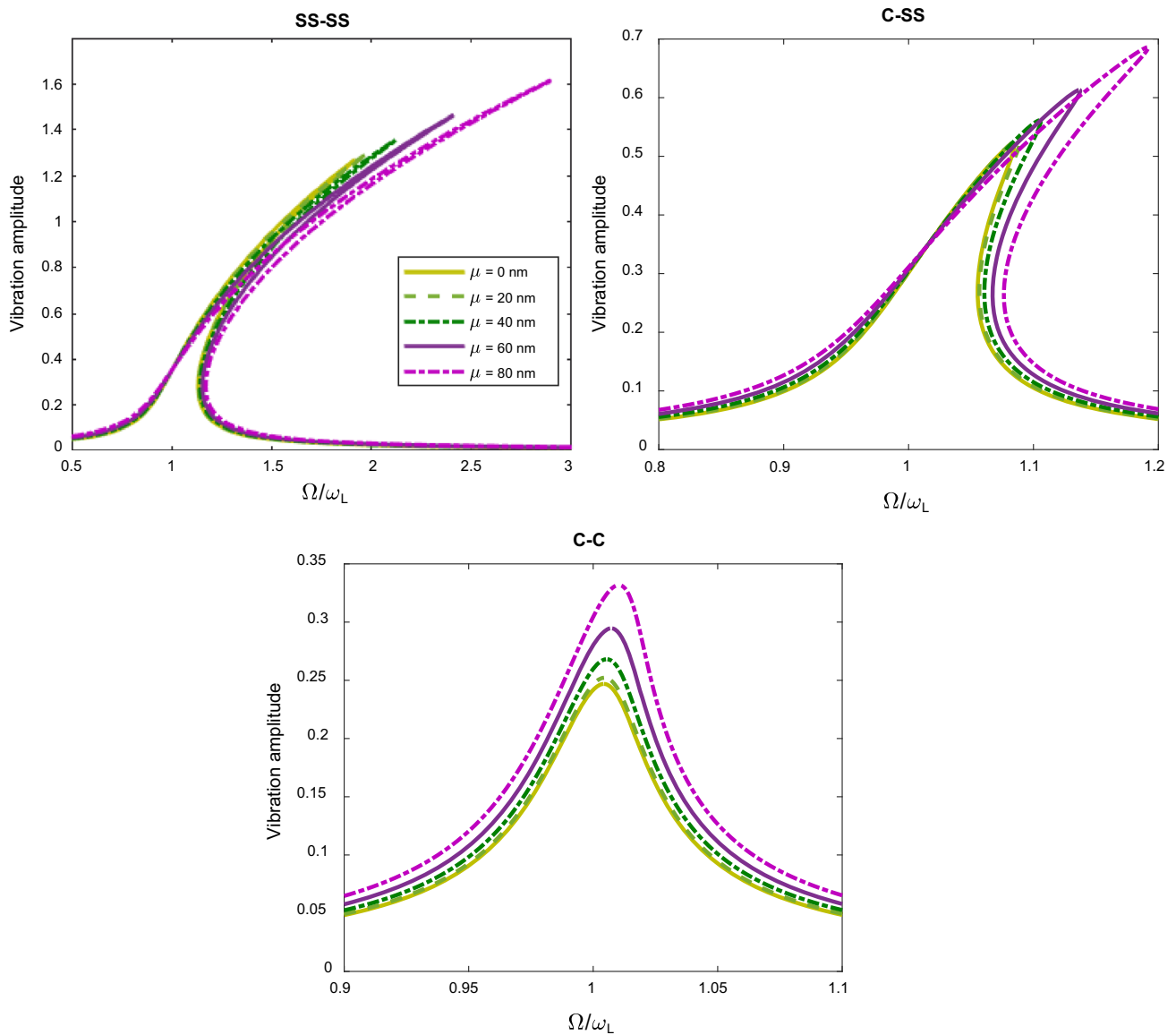


Fig. 2 Size-dependent frequency response of the soft excited FG-GPLRC laminated micro/nanobeams corresponding to different nonlocal parameters and boundary conditions ($Q = 0.01, U = \text{GPLRC}, V_{\text{GPL}} = 0.1, l = 0 \text{ nm}$)

simulation. As shown in Table 2, a very good agreement is found which confirms the validity of the given solution for the problem.

Figures 2 and 3 illustrate the nonlocal strain gradient frequency response of the harmonic excited FG-GPLRC laminated microbeams corresponding to different values of

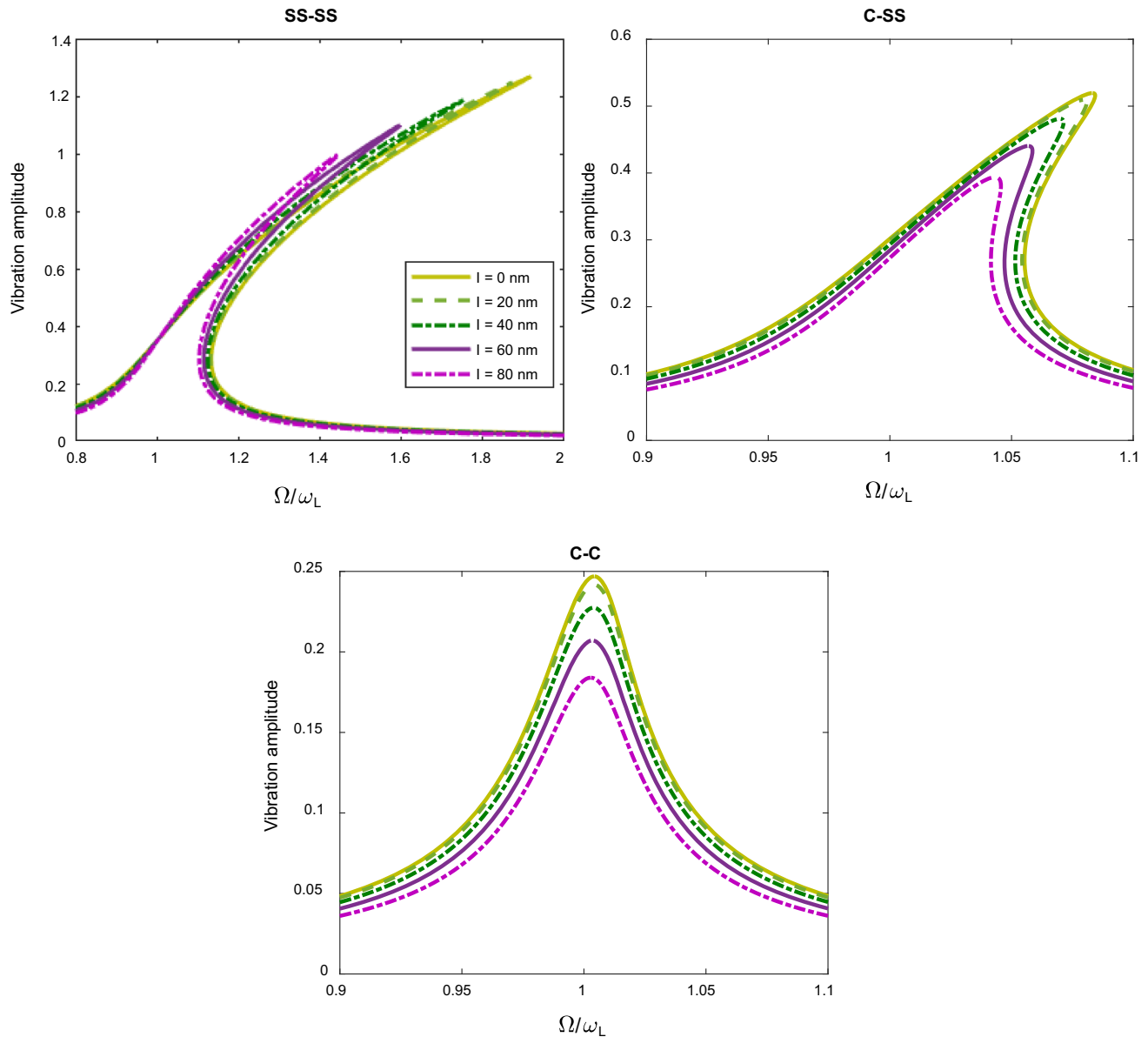


Fig. 3 Size-dependent frequency response of the soft excited FG-GPLRC laminated micro/nanobeams corresponding to different strain gradient parameters and boundary conditions ($Q = 0.01$, U – GPLRC, $V_{GPL} = 0.1$, $\mu = 0$ nm)

the nonlocal parameter and strain gradient parameter, respectively. It can be seen that the nonlocality size effect leads to an increase in the peak of the jump phenomenon in the vibration amplitude and it occurs at a higher excitation frequency. However, by changing the end supports from simply supported to clamped one, the significance of this pattern reduces. On the other hand, by taking the strain gradient size dependency into account, the peak of the jump phenomenon decreases and it is shifted to a lower excitation frequency. It is shown again that through changing the boundary conditions from simply supported–simply supported (SS–SS) to clamped–clamped (C–C),

these observations related to the strain gradient size effect become negligible.

Figures 4 and 5 display the nonlocal strain gradient amplitude response curves of the harmonic excited FG-GPLRC laminated microbeams corresponding to different values of the nonlocal parameter and strain gradient parameter, respectively. It is observed that by increasing the excitation amplitude, the vibration amplitude increases up to the first bifurcation point. After that, increment in the vibration amplitude continues via reduction in the value of excitation amplitude up to the second bifurcation point. It is found that the nonlocality causes a decrease in the excitation amplitudes associated with both the bifurcation

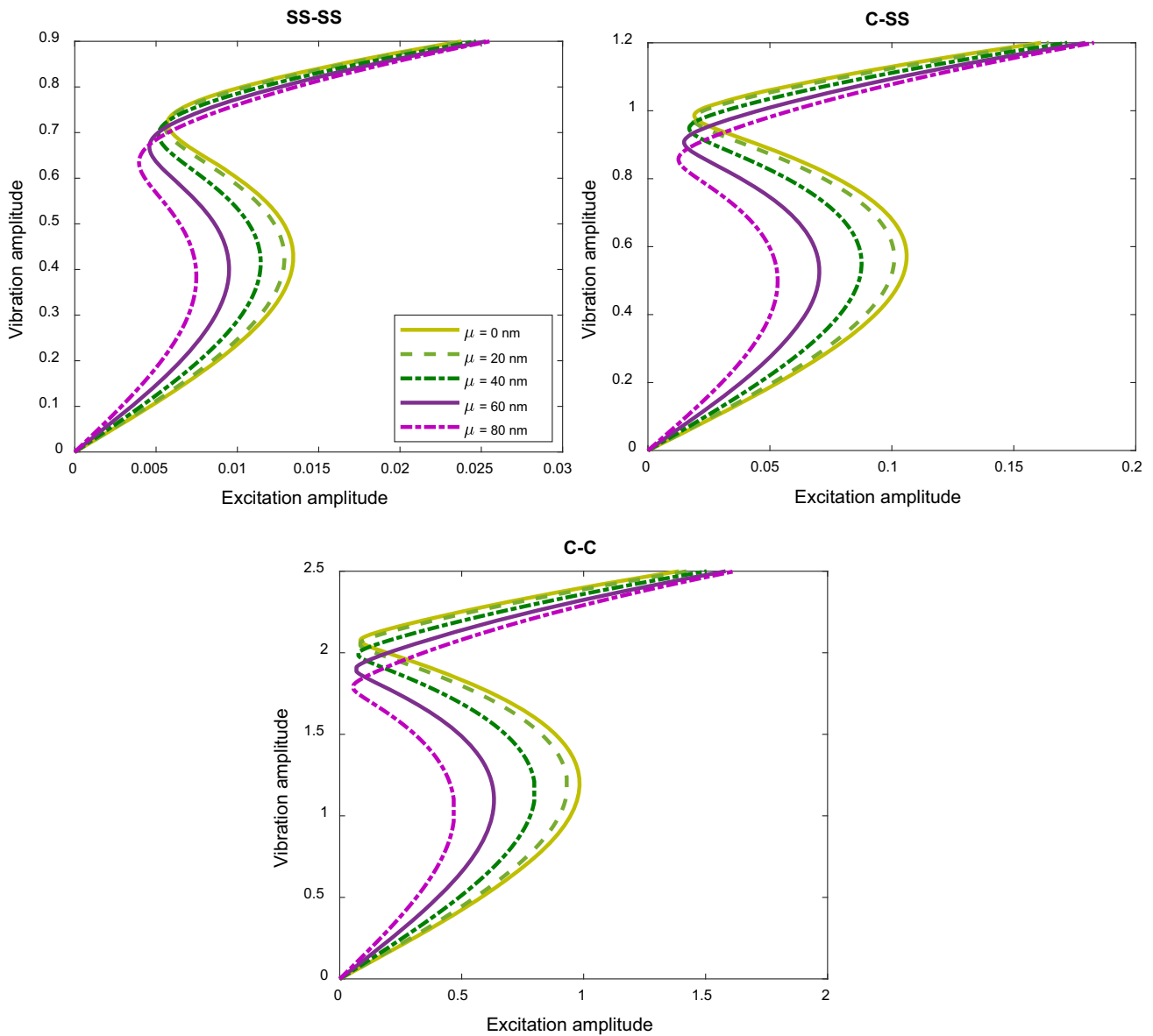


Fig. 4 Size-dependent amplitude response of the soft excited FG-GPLRC laminated micro/nanobeams corresponding to different nonlocal parameters and boundary conditions ($\Omega = 1.3\omega$, U – GPLRC, $V_{GPL} = 0.1$, $l = 0$ nm)

points, but its effect on the first one is more significant. However, the strain gradient size dependency has an opposite influence and leads to an increase. Furthermore, it is indicated that by changing the end supports from simply supported to clamped one, the influence of the nonlocality on the excitation amplitudes associated with the first and second bifurcation points increases and decreases, respectively. But for the strain gradient size dependency, its influence on the excitation amplitudes associated with both the bifurcation points reduces by changing the boundary conditions from SS–SS to C–C.

5 Concluding remarks

The prime aim of this investigation was to anticipate the nonlocal strain gradient nonlinear primary resonance of the harmonic excited FG-GPLRC laminated microbeams with different GPL dispersion patterns and various boundary conditions. To this purpose, the nonlocal strain gradient theory of elasticity was applied to the refined hyperbolic shear deformation beam theory to construct a more comprehensive size-dependent beam model. Via a numerical solving process, the nonlocal strain gradient frequency response and amplitude response are captured.

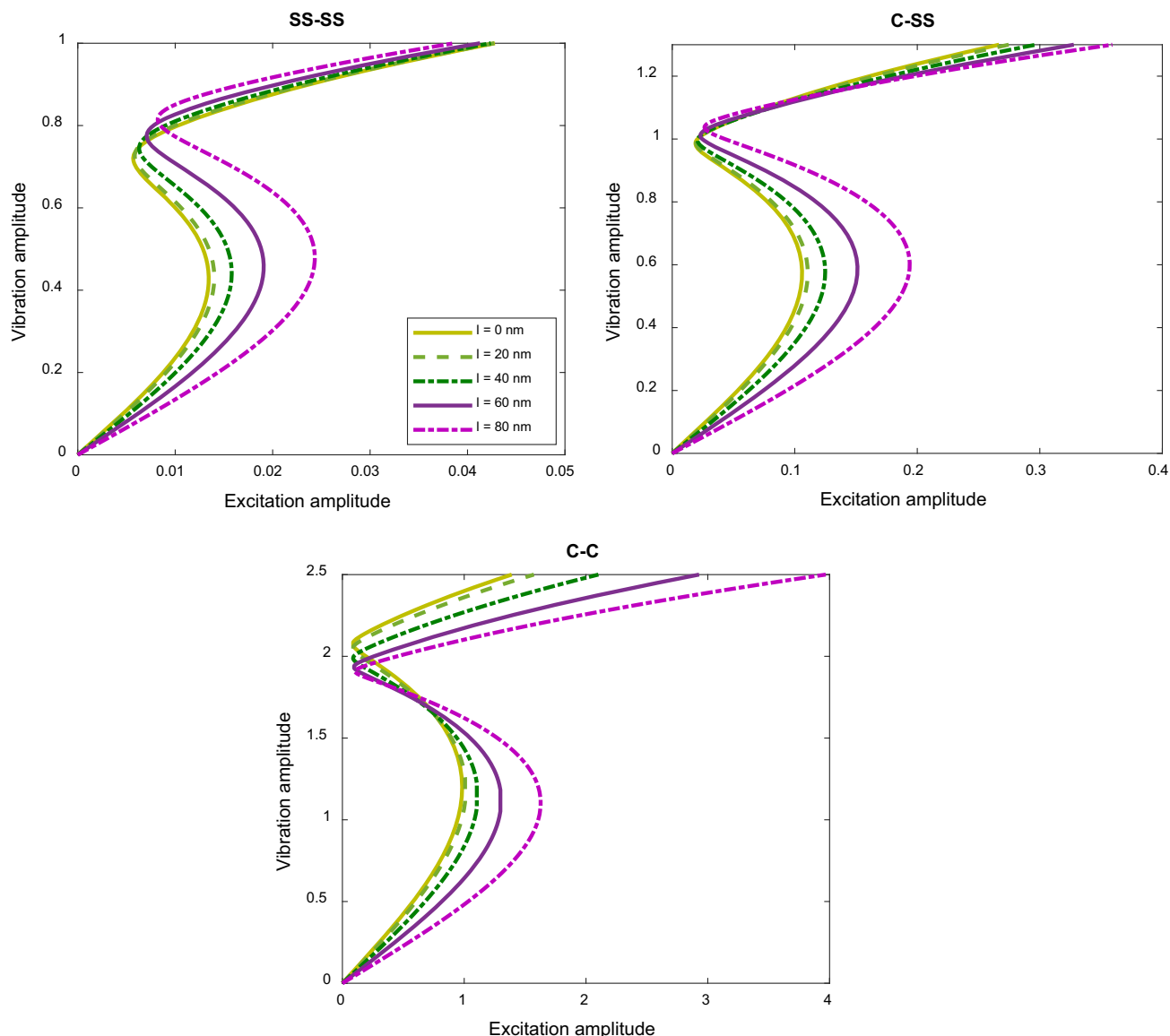


Fig. 5 Size-dependent amplitude response of the soft excited FG-GPLRC laminated micro/nanobeams corresponding to different strain gradient parameters and boundary conditions ($\Omega = 1.3\omega$, U – GPLRC, $V_{\text{GPL}} = 0.1$, $\mu = 0$ nm)

It was indicated that the nonlocality size effect leads to an increase in the peak of the jump phenomenon in the vibration amplitude and it occurs at a higher excitation frequency. However, by changing the end supports from simply supported to clamped one, the significance of this pattern reduces. On the other hand, by taking the strain gradient size dependency into account, the peak of the jump phenomenon decreases and it is shifted to a lower excitation frequency. It was observed that for all types of boundary conditions and GPL dispersion pattern, the significance of strain gradient size dependency on the linear frequency of the harmonic excited FG-GPLRC laminated microbeam is more than that of the nonlocal size effect. Moreover, it was seen that the nonlocality causes a

decrease in the excitation amplitudes associated with both the bifurcation points, but its effect on the first one is more significant. However, the strain gradient size dependency has an opposite influence and leads to an increase.

Acknowledgements This work was supported by the National Natural Science Foundation of China (NSFC) (No. 61705200).

References

1. Yang J, Wu H, Kitipornchai S (2017) Buckling and postbuckling of functionally graded multilayer graphene platelet-reinforced composite beams. *Compos Struct* 161:111–118

2. Song M, Kitipornchai S, Yang J (2017) Free and forced vibrations of functionally graded polymer composite plates reinforced with graphene nanoplatelets. *Compos Struct* 159:579–588
3. Feng C, Kitipornchai S, Yang J (2017) Nonlinear bending of polymer nanocomposite beams reinforced with non-uniformly distributed graphene platelets (GPLs). *Compos B Eng* 110:132–140
4. Wu H, Yang J, Kitipornchai S (2017) Dynamic instability of functionally graded multilayer graphene nanocomposite beams in thermal environment. *Compos Struct* 162:244–254
5. Fu Y, Du H, Zhang S (2003) Functionally graded TiN/TiNi shape memory alloy films. *Mater Lett* 57:2995–2999
6. Fu Y, Du H, Huang W, Zhang S, Hu M (2004) TiNi-based thin films in MEMS applications: a review. *Sens Actuators A* 112:395–408
7. Kahrobaiyan MH, Asghari M, Rahaeifard M, Ahmadian MT (2010) Investigation of the size-dependent dynamic characteristics of atomic force microscope microcantilevers based on the modified couple stress theory. *Int J Eng Sci* 48:1985–1994
8. Şimşek M, Reddy JN (2013) A unified higher order beam theory for buckling of a functionally graded microbeam embedded in elastic medium using modified couple stress theory. *Compos Struct* 101:47–58
9. Lei J, He Y, Zhang B, Gan Z, Zeng P (2013) Bending and vibration of functionally graded sinusoidal microbeams based on the strain gradient elasticity theory. *Int J Eng Sci* 72:36–52
10. Reddy JN, El-Borgi S, Romanoff J (2014) Non-linear analysis of functionally graded microbeams using Eringen's non-local differential model. *Int J Non Linear Mech* 67:308–318
11. Jung W-Y, Han S-C, Park W-T (2014) A modified couple stress theory for buckling analysis of S-FGM nanoplates embedded in Pasternak elastic medium. *Compos B Eng* 60:746–756
12. Shojaeian M, Tadi Beni Y (2015) Size-dependent electromechanical buckling of functionally graded electrostatic nanobridges. *Sens Actuators A* 232:49–62
13. Zhang B, He Y, Liu D, Shen L, Lei J (2015) Free vibration analysis of four-unknown shear deformable functionally graded cylindrical microshells based on the strain gradient elasticity theory. *Compos Struct* 119:578–597
14. Jung W-Y, Han S-C (2015) Static and eigenvalue problems of Sigmoid functionally graded materials (S-FGM) micro-scale plates using the modified couple stress theory. *Appl Math Model* 39:3506–3524
15. Sahmani S, Aghdam MM, Bahrami M (2015) On the free vibration characteristics of postbuckled third-order shear deformable FGM nanobeams including surface effects. *Compos Struct* 121:377–385
16. Kiani K (2016) Free dynamic analysis of functionally graded tapered nanorods via a newly developed nonlocal surface energy-based integro-differential model. *Compos Struct* 139:151–166
17. Akbarzadeh Khorshidi M, Shariati M, Emam SA (2016) Post-buckling of functionally graded nanobeams based on modified couple stress theory under general beam theory. *Int J Mech Sci* 110:160–169
18. Safaei B, Naseradinmousavi P, Rahmani A (2016) Development of an accurate molecular mechanics model for buckling behavior of multi-walled carbon nanotubes under axial compression. *J Mol Graph Model* 65:43–60
19. Sahmani S, Aghdam MM (2017) Imperfection sensitivity of the nonlinear axial buckling behavior of FGM nanoshells in thermal environments based on surface elasticity theory. *Int J Comput Mater Sci Eng* 6:1750003
20. Ziaee S (2017) The steady-state response of size-dependent functionally graded nanobeams to subharmonic excitation. *J Eng Math* 104:19–39
21. Tao C, Fu Y (2017) Thermal buckling and postbuckling analysis of size-dependent composite laminated microbeams based on a new modified couple stress theory. *Acta Mech* 228:1711–1724
22. Guo J, Chen J, Pan E (2017) Free vibration of three-dimensional anisotropic layered composite nanoplates based on modified couple-stress theory. *Phys E* 87:98–106
23. Sahmani S, Aghdam MM, Akbarzadeh A (2018) Surface stress effect on nonlinear instability of imperfect piezoelectric nanoshells under combination of hydrostatic pressure and lateral electric field. *AUT J Mech Eng* 2:177–190
24. Lu L, Guo X, Zhao J (2017) Size-dependent vibration analysis of nanobeams based on the nonlocal strain gradient theory. *Int J Eng Sci* 116:12–24
25. Sohi AN, Nieva PM (2018) Size-dependent effects of surface stress on resonance behavior of microcantilever-based sensors. *Sens Actuators A* 269:505–514
26. Attia MA, Abdel Rahman AA (2018) On vibrations of functionally graded viscoelastic nanobeams with surface effects. *Int J Eng Sci* 127:1–32
27. Sahmani S, Aghdam MM, Rabczuk T (2018) A unified nonlocal strain gradient plate model for nonlinear axial instability of functionally graded porous micro/nano-plates reinforced with graphene platelets. *Mater Res Express* 5:045048
28. Ghanati P, Safaei B (2019) Elastic buckling analysis of polygonal thin sheets under compression. *Indian J Phys* 93:47–52
29. Sahmani S, Fotouhi M, Aghdam MM (2019) Size-dependent nonlinear secondary resonance of micro-/nano-beams made of nano-porous biomaterials including truncated cube cells. *Acta Mech* 230:1077–1103
30. Safaei B, Moradi-Dastjerdi R, Chu F (2019) Effect of thermal gradient load on thermo-elastic vibrational behavior of sandwich plates reinforced by carbon nanotube agglomerations. *Compos Struct* 192:28–37
31. Lu L, Guo X, Zhao J (2019) A unified size-dependent plate model based on nonlocal strain gradient theory including surface effects. *Appl Math Model* 68:583–602
32. Safaei B, Moradi-Dastjerdi R, Qin Z, Chu F (2019) Frequency-dependent forced vibration analysis of nanocomposite sandwich plate under thermo-mechanical loads. *Compos B Eng* 161:44–54
33. Sahmani S, Safaei B (2019) Nonlinear free vibrations of bi-directional functionally graded micro/nano-beams including nonlocal stress and microstructural strain gradient size effects. *Thin Walled Struct* 140:342–356
34. Safaei B, Moradi-Dastjerdi R, Behdinin K, Chu F (2019) Critical buckling temperature and force in porous sandwich plates with CNT-reinforced nanocomposite layers. *Aerosp Sci Technol* 91:175–185
35. Safaei B, Moradi-Dastjerdi R, Qin Z, Behdinin K, Chu F (2019) Determination of thermoelastic stress wave propagation in nanocomposite sandwich plates reinforced by clusters of carbon nanotubes. *J Sandwich Struct Mater*. <https://doi.org/10.1177/1099636219848282>
36. Lim CW, Zhang G, Reddy JN (2015) A higher-order nonlocal elasticity and strain gradient theory and its applications in wave propagation. *J Mech Phys Solids* 78:298–313
37. Li L, Hu Y (2015) Buckling analysis of size-dependent nonlinear beams based on a nonlocal strain gradient theory. *Int J Eng Sci* 97:84–94
38. Li L, Hu Y (2016) Wave propagation in fluid-conveying viscoelastic carbon nanotubes based on nonlocal strain gradient theory. *Comput Mater Sci* 112:282–288
39. Yang WD, Yang FP, Wang X (2016) Coupling influences of nonlocal stress and strain gradients on dynamic pull-in of functionally graded nanotubes reinforced nano-actuator with damping effects. *Sens Actuators A* 248:10–21

40. Simsek M (2016) Nonlinear free vibration of a functionally graded nanobeam using nonlocal strain gradient theory and a novel Hamiltonian approach. *Int J Eng Sci* 105:10–21
41. Sahmani S, Aghdam MM (2017) Size-dependent axial instability of microtubules surrounded by cytoplasm of a living cell based on nonlocal strain gradient elasticity theory. *J Theor Biol* 422:59–71
42. Sahmani S, Aghdam MM (2017) Nonlinear vibrations of pre-and post-buckled lipid supramolecular micro/nano-tubules via nonlocal strain gradient elasticity theory. *J Biomech* 65:49–60
43. Sahmani S, Aghdam MM (2018) Nonlinear instability of hydrostatic pressurized microtubules surrounded by cytoplasm of a living cell including nonlocality and strain gradient microsize dependency. *Acta Mech* 229:403–420
44. Sahmani S, Aghdam MM (2018) Nonlocal strain gradient beam model for postbuckling and associated vibrational response of lipid supramolecular protein micro/nano-tubules. *Math Biosci* 295:24–35
45. Li L, Tang H, Hu Y (2018) Size-dependent nonlinear vibration of beam-type porous materials with an initial geometrical curvature. *Compos Struct* 184:1177–1188
46. Radwan AF, Sobhy M (2018) A nonlocal strain gradient model for dynamic deformation of orthotropic viscoelastic graphene sheets under time harmonic thermal load. *Phys B* 538:74–84
47. Wang J, Shen H, Zhang B, Liu J, Zhang Y (2018) Complex modal analysis of transverse free vibrations for axially moving nanobeams based on the nonlocal strain gradient theory. *Phys E* 101:85–93
48. Sahmani S, Aghdam MM (2017) A nonlocal strain gradient hyperbolic shear deformable shell model for radial postbuckling analysis of functionally graded multilayer GPLRC nanoshells. *Compos Struct* 178:97–109
49. Sahmani S, Aghdam MM (2017) Nonlinear instability of axially loaded functionally graded multilayer graphene platelet-reinforced nanoshells based on nonlocal strain gradient elasticity theory. *Int J Mech Sci* 131:95–106
50. Sahmani S, Aghdam MM (2017) Nonlocal strain gradient beam model for nonlinear vibration of prebuckled and postbuckled multilayer functionally graded GPLRC nanobeams. *Compos Struct* 179:77–88
51. Sahmani S, Aghdam MM (2017) Axial postbuckling analysis of multilayer functionally graded composite nanoplates reinforced with GPLs based on nonlocal strain gradient theory. *Eur Phys J Plus* 132:490
52. Zeighampour H, Tadi Beni Y, Dekhordi MB (2018) Wave propagation in viscoelastic thin cylindrical nanoshell resting on a visco-Pasternak foundation based on nonlocal strain gradient theory. *Thin Walled Struct* 122:378–386
53. Halpin JC, Kardos JL (1976) The Halpin-Tsai equations: a review. *Polym Eng Sci* 16:344–352
54. Hejazi SM, Abtahi SM, Safaie F (2016) Investigation of thermal stress distribution in fiber reinforced roller compacted concrete pavements. *J Ind Text* 45:869–914
55. Faghieh Shojaei M, Ansari R, Mohammadi V, Rouhi H (2014) Nonlinear forced vibration analysis of postbuckled beams. *Arch Appl Mech* 84:421–440
56. Liu F, Ming P, Li J (2007) Ab initio calculation of ideal strength and phonon instability of graphene under tension. *Phys Rev B* 76:064120
57. Rafiee MA, Rafiee J, Wang Z, Song H, Yu Z-Z, Koratkar N (2009) Enhanced mechanical properties of nanocomposites at low graphene content. *ASC Nano* 3:3884–3890
58. Sahmani S, Ansari R (2012) Small scale effect on vibrational response of single-walled carbon nanotubes with different boundary conditions based on nonlocal beam models. *Commun Nonlinear Sci Numer Simul* 17:1965–1979

Publisher's Note Springer Nature remains neutral with regard to jurisdictional claims in published maps and institutional affiliations.